

One-dimensional particle-in-cell simulation of a current-free double layer in an expanding plasma

Albert Meige,^{a)} Rod W. Boswell, and Christine Charles^{b)}

Space Plasma and Plasma Processing, Plasma Research Laboratory, Research School of Physical Sciences and Engineering, Australian National University, Australian Capital Territory, 0200, Australia

Miles M. Turner

Plasma Research Laboratory, School of Physical Sciences and National Centre for Plasma Science and Technology, Dublin City University, Dublin, Ireland

(Received 4 November 2004; accepted 2 March 2005; published online 5 May 2005)

A one-dimensional particle-in-cell code using Monte Carlo collision techniques (MCC/PIC) for both ions and electrons is used to simulate our earlier experimental results which showed that a current-free electric double layer (DL) can form in a plasma expanding along a diverging magnetic field. These results differ from previous experimental or simulation systems where the double layers are driven by a current or by imposed potential differences. Both experiment and simulation show accelerated ions with energies up to about 60 eV on the low potential side of the plasma. A new numerical method is added to the conventional PIC scheme to simulate inductive electron heating, as distinct from the more common capacitively driven simulations. A loss process is introduced along the axis of the simulation to mimic the density decrease along the axis of an expanding plasma in a diverging magnetic field. The results from the MCC/PIC presented here suggest that the expansion rate compared to the ionization frequency is a critical parameter for the existence of the DL. For the DL to be absolutely current free, the source wall has to be allowed to charge: having both ends of the simulation at the same potential always resulted in a current flow. Also, the effect of the neutral pressure and of the size of the diffusion chamber are investigated. Finally we show that this particular type of DL has electrons in Boltzmann equilibrium and that it creates a supersonic ion beam. © 2005 American Institute of Physics. [DOI: 10.1063/1.1897390]

I. INTRODUCTION

An electric double layer (DL) is a narrow localized region in a plasma which can sustain a large potential difference.¹ Alfvén suggested about 50 years ago that DLs could be responsible for the acceleration of electrons onto the upper atmosphere creating the visible aurora.² This hypothesis was then confirmed by later measurements within the aurora region.^{3,4} Since then, this phenomenon has been studied experimentally,^{5–14} theoretically,^{15–17} and by computer simulation.^{18–21} However, it is important to note that in most of these cases, the DL requires the presence of an electron current. If not it is generally imposed by a potential difference or by two different electron temperatures.

Perkins and Sun suggested over 20 years ago, by an analytical study, that a current-free double layer could exist.²² A number of papers followed showing ion acceleration in expanding current-free plasmas,^{23–26} but no clear evidence of double-layer formation was shown. Their existence had not been clearly experimentally verified until quite recently: Charles and Boswell^{27–29} have shown that a DL can be created in a current-free plasma expanding in a diverging magnetic field. These results have been later confirmed by similar experiments.^{30,31} The existence of current-free double

layers would free theoreticians of the need to find a current closure condition and would open the possibility of postulating a nonlinear field aligned dissipation mechanism. Such a mechanism would be of great help in explaining phenomena associated with solar chromospheric expansion, etc.^{32,33}

The current-free DL experiment was performed in a horizontal helicon system, *Chi-Kung*,^{27–29} shown in Fig. 1. It consists of a 15 cm diameter, 31 cm long helicon source joined contiguously to a 32 cm diameter, 30 cm long grounded aluminum diffusion chamber. Two solenoids around the source are used to create a magnetic field of about 130 G in the source center which decreases to a few tens of gauss in the diffusion chamber. The current-free DL can be generated for pressures less than about 1 mTorr (Ref. 27) and a supersonic ion beam has been measured downstream of this DL both for argon²⁹ and hydrogen²⁸ discharges.

Although DLs driven by currents (or imposed potential differences) have been studied by computer simulation since the early 1970s,^{19,20} the simulation described here is, to the best of our knowledge, the first numerical attempt to generate a current-free DL in an expanding plasma.

Particle-in-cell (PIC) is a purely kinetic representation of a system containing ions and electrons, considered as individual particles, which move under the influence of their own self-consistent electric field.^{34–37} In other words, PIC simulations use the first principles (Poisson's equation and Newton's laws) only. Each particle of the simulation is actually a macroparticle which is allowed to represent a large

^{a)}Joint thesis with the "Centre de Physique des Plasmas et de leurs Applications de Toulouse," CNRS, France. Electronic mail: albert.meige@anu.edu.au

^{b)}Also at the "Département de Sciences pour l'Ingenieur," CNRS, France.

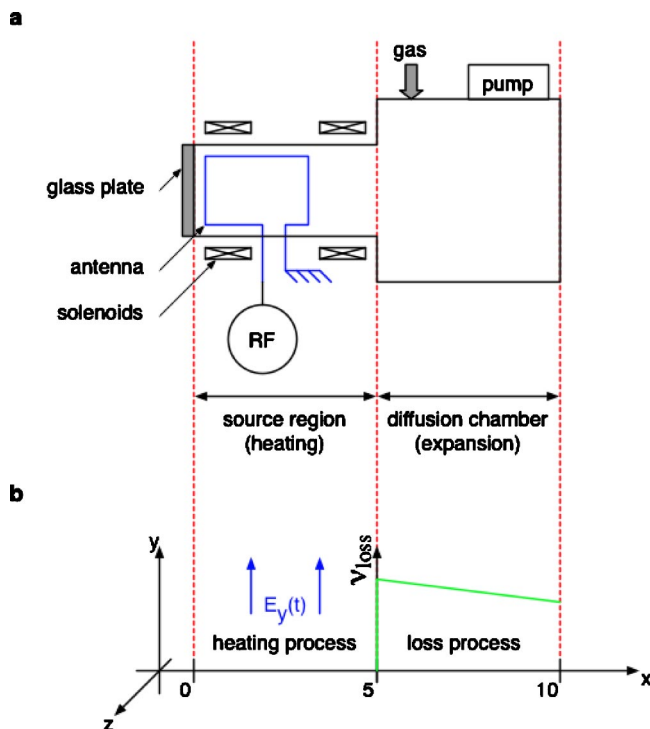


FIG. 1. Experimental and numerical setup. (a) Schematic of *Chi-Kung* a horizontal helicon system (Refs. 27–29). (b) one-dimensional numerical model of an expanding plasma. In both (a) and (b), the electrons are heated in the source region, i.e., upstream. In (b), this is done by a uniform rf electric field at 10 MHz perpendicular to the resolution axis of the simulation. The plasma expands in the diffusion chamber, i.e., downstream. In (a), this is obtained by an expanding magnetic field, while in (b), the on-axis expansion is modeled by a loss process that removes charged particles at a given loss frequency.

number of real particles (on the order of 10^9 or 10^{10} particles per macroparticle per square meter) and which can move inside the simulated domain. With a small number of these macroparticles [typically between 10^4 and 10^5 for a one-dimensional (1D) system], a realistic steady-state plasma can be obtained in a few hours on a modern desk top computer.

The particular PIC simulation developed here consists of a bounded one-dimensional plasma where a planar geometry is assumed. The potential of the left wall floats, whereas the right wall is grounded to respect the experimental setup (Fig. 1). The left wall is allowed to float by placing a capacitor in series with the plasma. Even if the simulation is one-dimensional (the position of the particles is resolved along the x axis), the collisions are modeled with three dimensions of velocities, hence the model is called 1D-3V. Our code, which is called *JanuS*, implements the Monte Carlo collision (MCC) model, including the *null collision*³⁸ method, developed by Vahedi and Surendra,³⁹ and handles electron-neutral collisions (elastic, exciting, and ionizing) and ion-neutral collisions (charge exchange and elastic). High energy electron-neutral collision scattering angles are very small (forward scattering), whereas low energy electron-neutral collisions are isotropic. At high energy (more than 1 eV) ion-neutral charge exchange collisions are predominant and are anisotropic in the center-of-mass frame. At low energy,

ion-neutral elastic collisions are dominant and are isotropic in the center-of-mass frame.

II. SIMULATION OF AN “INDUCTIVELY” HEATED PLASMA

One-dimensional PIC simulations are commonly concerned with capacitive coupling, where a rf voltage of some hundreds of volts is applied to one of the boundaries. This mechanism has been thoroughly studied^{40–42} and creates a moving sheath that heats the electrons. The drawback of this process is that it leads to an average rectified plasma potential that is in the order of half the rf amplitude. Our aim is to study a potential drop of only a few tens of volts (Sec. III), which is extremely small compared to the rectified potential from a capacitively heating process. Hence, it is inappropriate for the present study. Therefore, we have developed a mechanism to heat the electrons differently. The “new” heating mechanism is described below in detail and a study of its effects is conducted in a nonexpanding plasma to show that it does not introduce any noticeable pathologies in the plasma potential or in the electron transport.

A. Electron heating model

This scheme is intended to model “inductive” excitation, but without solving electromagnetic field equations. In addition to avoiding the rf excursions of the potential in the plasma introduced by a capacitive coupling, the “inductive” scheme was considered to be closer to the experimental conditions than other possible algorithms: an rf electric field (E_y) of $\omega_0/2\pi=10$ MHz is applied in the source region in the direction normal to the PIC axis (Fig. 1). Note that a frequency of 10 MHz was used in this work in order to have a finite number of time steps per rf cycle and to be close to the frequency used in the laboratory experiments (13.56 MHz). The electric field amplitude was chosen not to be constant in time to avoid electron overheating: with a constant electric field amplitude the work done by the electric field would depend on the electron density and would eventually lead to an unstable simulation. Therefore, the current density amplitude (J_0) was chosen to be the control parameter that fixes the electric field amplitude and was chosen to be uniform in the source region. The total current density at each point of the source region is then

$$J_{\text{total}} = J_{\text{displacement}} + J_{\text{conduction}}, \quad (1)$$

$$J_{\text{total}} = J_0 \sin(\omega_0 t) = \epsilon_0 \frac{\partial E_y}{\partial t} + e \Gamma_{e,y}, \quad (2)$$

where $\Gamma_{e,y}$ is the electron flux along the y axis and is equal to

$$\Gamma_{e,y} = n_e \overline{v_{e,y}} = \frac{N_\sigma}{L_{\text{source}}} \sum_{i \in \text{source}} v_{e,y,i}, \quad (3)$$

where $\overline{v_{e,y}}$ is the average electron velocity along y in the source region, $v_{e,y,i}$ the y velocity component of the i th electron, N_σ the weight of a macroparticle per square meter, and L_{source} the length of the source. Equation (2) is then integrated over the source region

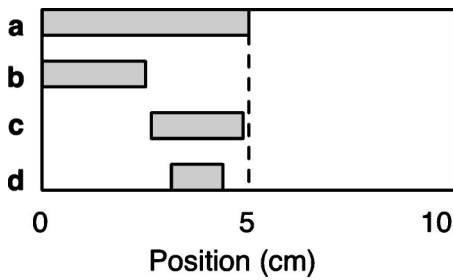


FIG. 2. Illustration of the heating process in the simulation, where the gray areas represent the different heating regions studied.

$$\int_{\text{source}} J_{\text{total}} dx = L_{\text{source}} J_0 \sin(\omega_0 t), \quad (4)$$

$$\int_{\text{source}} J_{\text{displacement}} dx = L_{\text{source}} \epsilon_0 \frac{\partial E_y}{\partial t}, \quad (5)$$

$$\int_{\text{source}} J_{\text{conduction}} dx = e N_{\sigma} \sum_{i \in \text{source}} v_{e,y,i}, \quad (6)$$

and rearranged into

$$\frac{\partial E_y}{\partial t} = \frac{1}{\epsilon_0} \left[J_0 \sin(\omega_0 t) - \frac{e N_{\sigma}}{L_{\text{source}}} \sum_{i \in \text{source}} v_{e,y,i} \right]. \quad (7)$$

The perpendicular electric field $E_y(t)$ is evaluated using the finite difference corresponding to Eq. (7) and the previous time-step value $E_y(t-1)$.

Note that we have chosen to make the heating process anisotropic and act only on the y axis instead of being isotropic in the plane perpendicular to the x axis. An advantage of this scheme is that the computational cost is comparatively low and since the simulation handles electron-neutral collisions in three dimensions, the momentum and energy given to the electrons in the y direction are eventually transferred (at least partially) to the other directions. In other words, if the electron-neutral collisions are “turned off” in the simulation, this heating process is ineffective.

B. Study of the effects of the heating mechanism

In order to test the perturbations introduced by our new heating technique, a set of simulations was conducted where the heating region was localized in the left half of the system (0–5 cm) and where no expansion process was applied (Sec. III).

Figure 2 shows the different positions of the heating process tested in the simulation. A neutral pressure of 1 mTorr and an electron density of $2 \times 10^{15} \text{ m}^{-3}$ were used. The current density in the heating mechanism was 100 A/m^2 and the rf frequency was 10 MHz. Figure 3 shows that the plasma potential is little affected by the position of the heating region. Indeed, for relatively large source regions, e.g., a quarter of the system, the profile of the plasma potential is not noticeably affected: the potential is the same in the diffusion chamber and in the source. However, if the heating

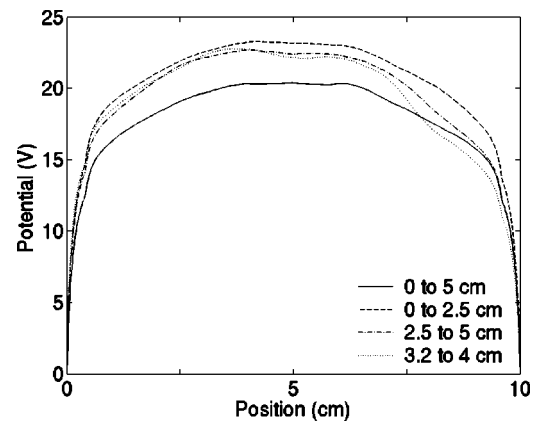


FIG. 3. Steady-state plasma potential profiles along the axis of the simulation; the heating positions are shown in Fig. 2.

region is sufficiently small, the plasma potential is somewhat higher on the side of the heating region, which is shown by the dotted line.

The effect on the plasma potential of pressures from 0.5 mTorr to 5 mTorr and where the heating source is located only in the first quarter of the simulation [Fig. 2, case (b)] is shown in Fig. 4. The solid and dashed lines represent the plasma potential for 0.5 mTorr and 1 mTorr, respectively. Despite the fact that the heating source is located in the first quarter of the simulation, the plasma diffuses sufficiently that the potential is uniform in the source and the diffusion chamber. For higher pressures, e.g., 5 mTorr (dotted-dashed line), the plasma does not diffuse as much, the plasma potential is therefore affected and it is higher in the source region than in the diffusion chamber, which is presumably due to the electron temperature decreasing away from the source.

Here we study how the heating source, localized in the left-hand side of the simulation [Fig. 2, case (a)] affects the electron transport for a neutral pressure of 1 mTorr. Figure 5 shows the logarithm of the electron velocity distribution as a function of the electron energy at different positions. The logarithm of the electron distribution can be linearly fitted for energies up to 20 eV with an average relative error on the fit of less than 1%. In other words, the percentage of Max-

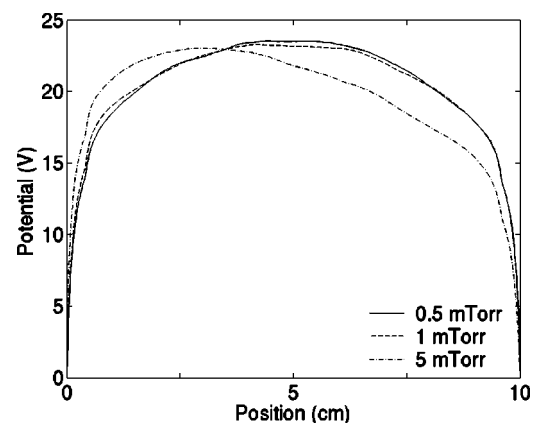


FIG. 4. Steady-state plasma potential profiles along the axis of the simulation for different neutral pressures. The heating region is located in the first quarter of the system, from 0 to 2.5 cm, Fig. 2(b).

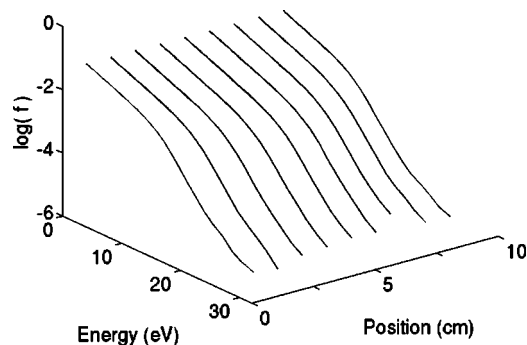


FIG. 5. Electron velocity distribution (log scale) as a function of the electron energy at different axial positions in the plasma.

wellian electrons in the bulk is more than 99%. The spatially resolved electron distribution shows that the distribution is uniform in the bulk (uniform temperature) despite the localized heating region.

In summary, we have shown that the source position and extent do not have any particular effect on the plasma potential and the electron transport for pressures below 1 mTorr. The small percentage of electrons with energy higher than the bulk are not Maxwellian. Their evolution and energy where they join the bulk electrons is currently being studied in depth and will be presented in a future publication.

III. SIMULATION OF AN EXPANDING PLASMA

A. Plasma expansion model

Seen from the axis, the expansion of a plasma in a diverging magnetic field can be considered as a process in which particles are removed from the system at a given frequency (ν_{loss}) which depends on their position, where the loss frequency is the probability of removing a particle from the simulation per unit of time. This loss process produces an axial decrease in the plasma density and an associated potential drop. Figure 1, case (b), shows one of the loss-process profiles which has been investigated: particles are removed more or less suddenly with a given frequency from the beginning of the diffusion chamber (sudden expansion due to the magnetic field and/or the geometry of the plasma source/diffusion chamber system) and then the loss frequency is constant or decreasing when moving in the direction of the right wall (equivalent to a constant volume and a less divergent magnetic field). A more realistic method would have been to carry out a full two-dimensional PIC with magnetic field but for us this would have been prohibitively expensive in both computers and run time. Nevertheless, we show below that the loss algorithm produces density and potential profiles in our 1D PIC which are quite similar to the experimental results.

B. Study of the influence of different parameters

In this section, we study the influence of the expansion rate and profile, the size of the diffusion chamber, and the neutral pressure. The results presented here were obtained using the set of standard conditions given in Table I.

TABLE I. Standard parameters of the simulation.

Quantity	Value
Neutral pressure	1 mTorr
Electron density	$6 \times 10^{14} \text{ m}^{-3}$
rf frequency ($\omega_0/2\pi$)	10 MHz
Current density amplitude (J_0)	100 A/m^2
System length	10 cm
Cell number	250
Total duration	$25 \mu\text{s}$
Time step	$5 \times 10^{-11} \text{ s}$
Macroparticle weight (N_σ)	$4 \times 10^9 \text{ m}^{-2}$
Ion mass (argon)	6.68×10^{-26}
Room temperature	297 K
Capacitance	22 nF

1. Development of the steady state

The simulation is initiated by loading a certain number of macroparticles (electrons and ions) between the floating left wall and the earthed right wall. After the loading, the simulation evolves in time and space and if the conditions of stability and accuracy of the PIC simulation are respected,^{36,37} a steady state is eventually reached.

Figure 6 shows the density and potential profiles of a current-free DL obtained with a loss frequency slightly greater than the creation frequency (i.e., ionization frequency) for the standard parameters. Note that the plasma

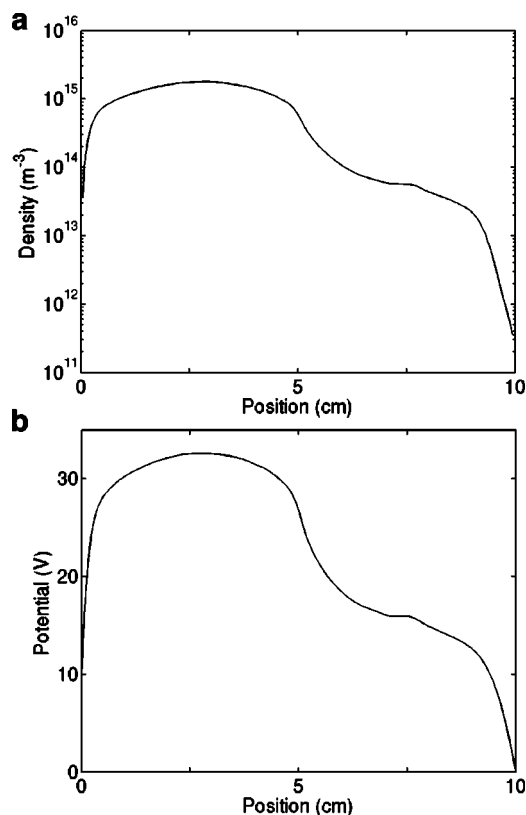


FIG. 6. Typical PIC simulated double-layer profiles: (a) steady-state electron density and (b) steady-state plasma potential as a function of the axial position.

density and potential profiles are averaged over 10 rf cycles and given with respect to the grounded wall. The electron density decreases by an order of magnitude when passing from the source region (upstream plasma) to the diffusion chamber (downstream plasma). A charging of the source of about 10 V is obtained. The potential drop associated with the density drop is 12 V. Within the DL, the neutrality of the plasma breaks down, and the upper and lower limit of the non-neutral region were used to precisely determine the position of the DL and evaluate the density and potential drop. Commonly, DLs are characterized by the ratio $e\Phi_{DL}/kT_e$ and the thickness over which the potential drop occurs. In this case $e\Phi_{DL}/kT_e \sim 2.7$ (where T_e is average ‘‘Boltzmann’’ temperature obtained in Sec. III C 1). The DL thickness is less than 20 Debye lengths.

Here we show that an adaptation to our case of the classical derivation of the sheath potential (Ref. 42, p. 160) is in good agreement with $e\Phi_{DL}/kT_e$ measured above. Let $\Delta\Gamma$ be

$$\Delta\Gamma = \Gamma_e - \Gamma_i, \quad (8)$$

where Γ_e and Γ_i are the electron and ion fluxes through a plane located at the downstream edge of the DL, respectively. The ions are assumed collisionless in the DL since the mean free path for these conditions is ≈ 3 cm, which is much larger than the DL thickness. The ions are supposed to enter the sheath with the sound speed velocity (also called Bohm velocity)

$$c_s = \sqrt{\frac{kT_e}{m_i}}, \quad (9)$$

where m_i is the ion mass. The ion flux is then given by

$$\Gamma_i = anc_s, \quad (10)$$

with n being the downstream density and an the upstream density. The electrons are assumed to be Maxwellian (discussed in Sec. III C 1) and their net flux is given by the sum of the flux coming from the upstream side and the flux coming from the downstream side:

$$\Gamma_e = \frac{1}{4}nv_e \left[\alpha \exp\left(-\frac{e\Phi_{DL}}{kT_e}\right) - 1 \right], \quad (11)$$

with

$$\bar{v}_e = \sqrt{\frac{8kT_e}{\pi m_e}} \quad (12)$$

and Φ_{DL} the potential drop. By substituting Eqs. (10) and (11) into Eq. (8) and rearranging, we obtain

$$\frac{e\Phi_{DL}}{kT_e} = -\ln\left(\gamma + \sqrt{\frac{2\pi m_e}{m_i}} + \frac{1}{\alpha}\right), \quad (13)$$

where γ is the ratio between the net current and the upstream electron current, given by

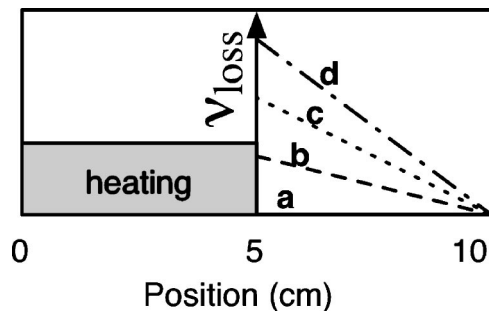


FIG. 7. Illustration of the different expansion rate, i.e., loss frequency applied in the simulation. The source region is located in the first half of the system, the loss process in the second half. (a) $\nu_{\text{loss}}=0$. (b) $\nu_{\text{loss}}=10^4 \text{ s}^{-1}$. (c) $\nu_{\text{loss}}=10^5 \text{ s}^{-1}$. (d) $\nu_{\text{loss}}=10^6 \text{ s}^{-1}$.

$$\gamma = \frac{\Delta\Gamma}{\Gamma_{e,\text{upstream}}} = \frac{\Delta\Gamma}{\frac{1}{4}anv_e}. \quad (14)$$

In the present case, the double layer is current free (which will be discussed later), hence, there are equal fluxes of ions and electrons, γ is therefore equal to zero. In addition, for $\alpha \ll 100$, Eq. (13) can be approximated to

$$\frac{e\Phi_{DL}}{kT_e} \sim \ln \alpha. \quad (15)$$

On the other hand, when α becomes infinite, that is to say when there is no downstream plasma, the asymptote of Eq. (13) is the classical wall sheath potential, where $e\Phi_{DL}/kT_e \sim 4.7$ for argon. For the DL shown above (Fig. 6), $\alpha=15$, which leads to a ratio $e\Phi_{DL}/kT_e=2.7$, which is in very good agreement with the value measured in the simulation and the experiment.²⁷

2. Study of the influence of expansion profile

Experimentally, Charles and Boswell have shown that the magnetic field is a critical parameter concerning the existence of the DL.²⁷ In our model, the shape and the amplitude of the loss process are directly related to the magnetic field of the experiment. Therefore, the influence of the loss process is a parameter which has to be studied in detail.

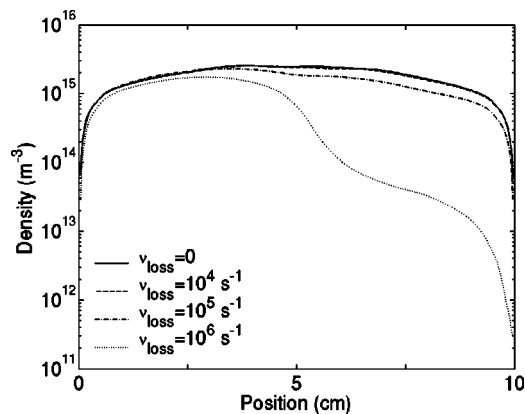


FIG. 8. Electron density as a function of the axial position, obtained for the different loss frequencies shown in Fig. 7, at a pressure of 1 mTorr.

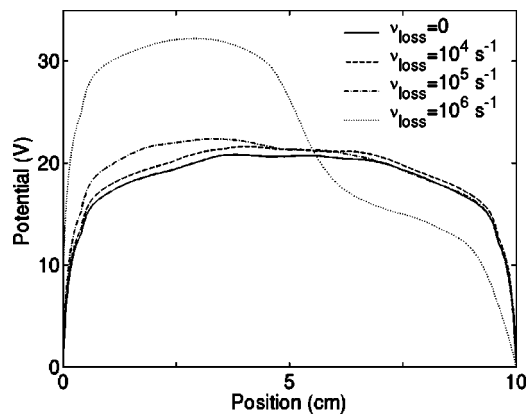


FIG. 9. Plasma potential as a function of the axial position, obtained for the different loss frequencies shown in Fig. 7, at a pressure of 1 mTorr.

A series of simulations was performed with the standard parameters having different loss frequencies varying from 0 to 10^7 s^{-1} (Fig. 7) and for different pressures (0.1, 1, and 10 mTorr). Figures 8 and 9 show that no DL (i.e., no dramatic density or potential drop) is created for frequencies below a certain threshold (discussed in detail below). Figure 9 shows that the plasma potential does not drop for a loss frequency of 10^4 s^{-1} (dashed line) and that it drops slightly for 10^5 s^{-1} (dotted-dashed line). For a loss frequency of 10^6 s^{-1} (dotted line) a potential drop around 12 V is observed over a distance of about 20 Debye lengths. To explain the sudden appearance of the DL above the critical threshold, the potential drop was studied as function of the loss frequency, normalized to the ionization frequency for different pressures with the ionization frequency being determined by

$$\nu_{\text{ion}} = n_n \langle \sigma v \rangle = n_n R, \quad (16)$$

where ν_{ion} is the ionization frequency, n_n the neutral density, σ the ionization cross section, v the electron velocity, and R the rate coefficient. The temperatures, the rate coefficients, and the corresponding ionization frequencies for the different pressures are given in Table II. Figure 10 represents the potential drop as a function of the loss frequency normalized to the corresponding ionization frequency for different pressures. For loss frequencies smaller than the ionization frequency, no potential drop is created. However, if the loss frequency is of the order of or greater than the ionization frequency then a potential drop proportional to the logarithm of the loss frequency is created.

A series of simulations was performed with the standard parameters (Table I) to study the importance of the charging of the source on the current-free double layer. Figure 11

TABLE II. Electron temperatures (T_e), rate coefficients (R) and ionization frequencies (ν_{ion}), for different neutral pressures (P), the other parameters being constant.

P (mTorr)	0.1	1	10
T_e (eV)	38	6	4
$R (\times 10^{-15} \text{ m}^3/\text{s})$	100	5	1
$\nu_{\text{ion}} (\times 10^5 \text{ Hz})$	3.3	1.6	3.3

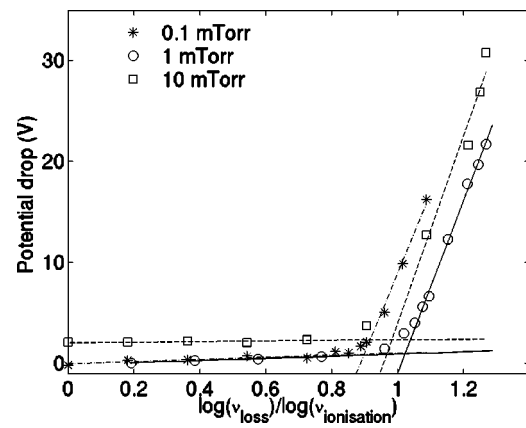


FIG. 10. Double-layer potential drop as a function of the loss frequency.

shows the steady-state source end wall potential when the boundary is allowed to charge (floating boundary condition) for different loss frequencies (normalized to the ionization frequency) and pressures. When the loss frequency is smaller than the ionization frequency, the source does not charge up, but, when the loss frequency becomes the order of or greater than the ionization frequency, the source wall charges up to a few volts.

The plasma potential obtained for identical parameters is shown in Fig. 12. The source end wall is floating in one case (dashed line), while it is grounded in the other case (solid line). For both cases the profiles and potential drops are very close. However the sheath on the right boundary is very low for the grounded source end wall case (solid line), which indicates that the electrons are not confined as much as in the floating source end wall case and that an electron current may flow. A diagnostic on both boundaries shows that in the floating source end wall case there is no current flowing through the system, the DL is current free. By assuming that the temperature is uniform in the system, the electrons are in Boltzmann equilibrium (which is discussed in Sec. III C 1), and the ions enter the left sheath at the sound velocity and the right sheath at an average velocity of v_i , we can show why the wall charges up to the potential Φ_w . If α is the

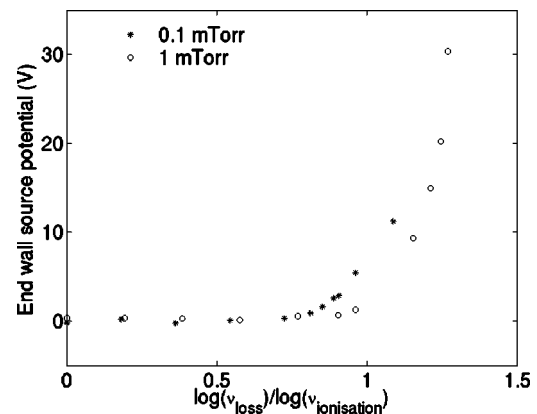


FIG. 11. Potential of the source end wall at 0 cm, as a function of the loss frequency.

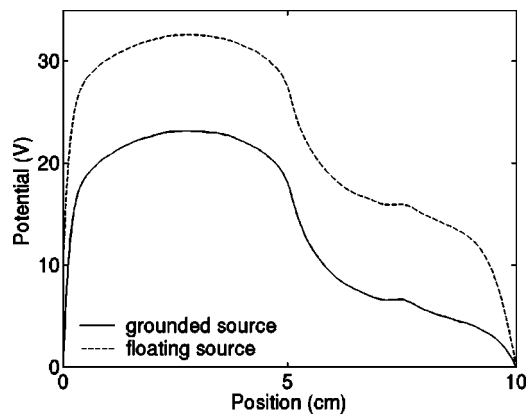


FIG. 12. Plasma potential profile as a function of the axial position. The solid and dashed lines represent the grounded and floating source end wall, respectively.

upstream and downstream density ratio, the flux conservation equations at the boundaries and downstream of the DL [Eq. (15)] lead to

$$\frac{e\Phi_w}{kT_e} \sim \ln\left(\alpha \frac{c_s}{v_i}\right) \leq \frac{e\phi_{DL}}{kT_e}. \quad (17)$$

If both walls are grounded, a small electron current flows through the system from the source to the diffusion chamber. For a pressure of 1 mTorr, an average electron density of $7 \times 10^{14} \text{ m}^{-3}$ and a loss frequency of 10^6 s^{-1} , the measured current density averaged on $7.5 \mu\text{s}$ is 0.21 A/m^2 . The term γ , introduced in Eq. (13), has in this case a finite value, but it is still an order of magnitude less than $1/\alpha$. Therefore its contribution to the potential drop is negligible: the DL is not current free anymore, although the DL is not driven by this current.

As we are artificially creating a particle loss to mimic the expansion of the plasma in a magnetic field, it is important to investigate the length scale over which the loss frequency rises to its maximal value (i.e., the expansion length). Figures 13 and 14 the electron density and the plasma potential for the different spatial expansion lengths as shown in Fig. 15. For the finite expansion lengths [cases (b), (c) and (d)], the thickness of the DL corresponds to the actual expansion

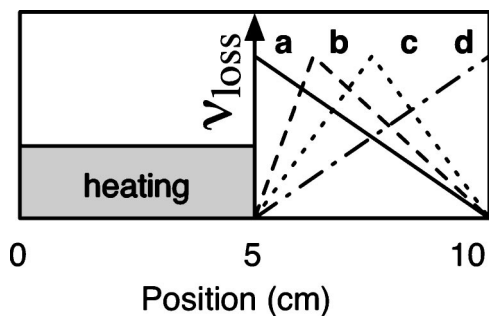


FIG. 13. Illustration of the different expansion length (i. e., loss profile) studied in the simulation. The loss frequency is null in the source. (a) The loss frequency jumps suddenly to its maximal value (10^6 s^{-1}). (b) The loss frequency reaches its maximal value after 2 cm from the beginning of the diffusion chamber. (c) After 3 cm. (d) After 5 cm (end of the diffusion chamber).

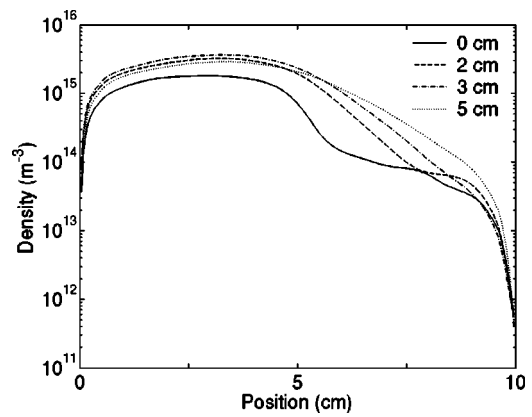


FIG. 14. Electron density as a function of the axial position, obtained for the different loss profiles shown in Fig. 13.

length. On the other hand, it is interesting to note that despite a null expansion length [case (a)], the DL has a finite thickness of ≈ 20 Debye lengths. Despite an extensive investigation, the thickness of the DL could not be reduced further.

In summary, the study of the loss-process parameters has shown that both, the amplitude and the profile of the expansion rate (related to the magnetic field and/or to the geometry of the plasma reactor in the experiment) are critical parameters concerning the existence of the DL. In addition, we saw that the double layer we create in an expanding plasma is current free when the source end wall is floating. These results differ from previous experimental^{13,43} or simulation¹⁹⁻²¹ systems in which the DL is driven by a current or imposed by a potential difference.

3. Study of the influence of the length of the diffusion chamber and the neutral pressure

Figures 16 and 17 show the electron density and the plasma potential profiles for different right wall positions as shown in Figure 18 (from 2.5 cm to 10 cm from the DL). First, it is interesting to notice that the position of the DL is not affected by the position of the right grounded wall. Second, the nonsolid lines in Fig. 17 show that, if the right wall is far enough from the DL, i.e., a few ion mean free paths,

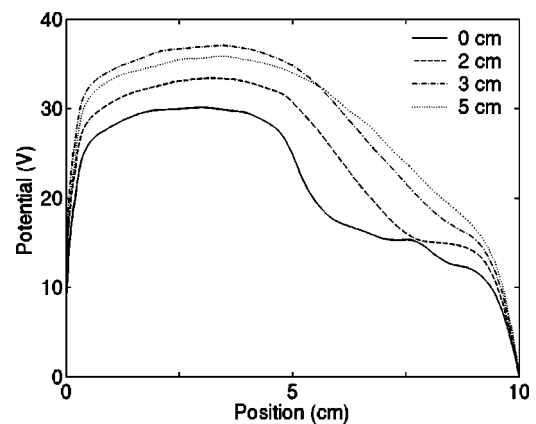


FIG. 15. Plasma potential as a function of the axial position, obtained for the different loss profiles shown in Fig. 13.

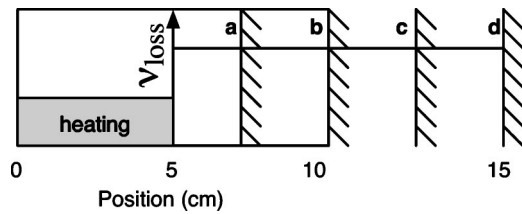


FIG. 16. Illustration of the different diffusion chamber sizes studied in the simulation: the right boundary is moved from 2.5 cm from the DL to 10 cm from the DL.

then its position does not seem to have any influence on the potential profile: the wall was even moved 50 cm away from the DL, and the plasma potential as well as the potential drop did not present any significant differences. By extrapolation, we can suppose that the right wall can be moved away from the current-free double layer indefinitely without changing its properties. On the other hand, if the right wall is close enough from the DL (less than an ion mean free path), then the average velocity of the ions entering the sheath [v_i , introduced in Eq. (17)] is greater than the sound speed, which is due to the ions accelerated through the DL (Sec. III C 2). As a consequence of the current-free condition, and as is shown by Eq. (17), having $v_i \geq c_s$ produces a decrease of the left wall potential (Φ_w), and therefore a decrease of the whole potential profile. This is visible by the solid line in Fig. 17, where the whole plasma potential profile is shifted down by a few volts with respect to the other profiles.

The evolution of the potential drop as a function of the neutral pressure is shown in Fig. 19. Both, the downstream and upstream plasma potentials are maximum for a neutral pressure of 0.2 mTorr, but the maximal potential drop for the DL occurs for a neutral pressure of 0.1 mTorr. When the pressure is increased, the potential drop decreases slightly. However, above 1 mTorr, the potential drop starts increasing again, and this is presumably an artifact of the localized heating mechanism: Recall from Sec. II B that, above a few millitorrs, the plasma potential is higher on the side of the heating region than on the other side. In other words, above a few millitorrs, the heating process starts having a significant

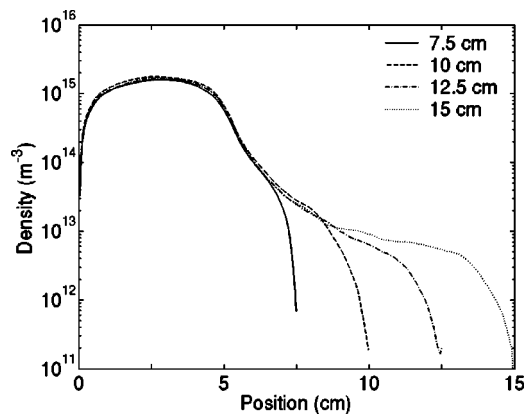


FIG. 17. Electron density as a function of the axial position, obtained for the different right wall positions shown in Fig. 16.

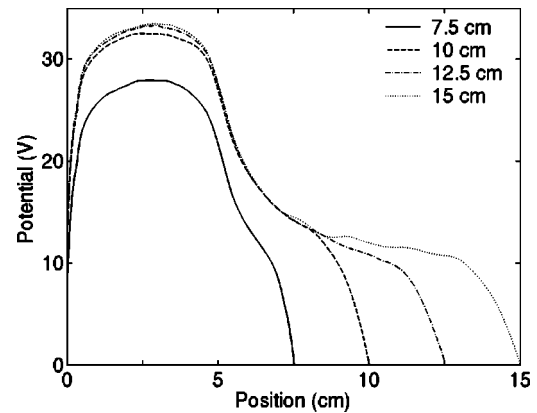


FIG. 18. Plasma potential as a function of the axial position, obtained for the different right wall positions shown in Fig. 16.

effect on the properties of the DL. However, in the pressure range that was simulated, the potential drop seems to be weakly dependent on the neutral pressure.

C. Particle transport in the current-free double layer

1. Maxwell-Boltzmann electrons distribution

The electron velocity distribution has been determined along the length of the simulation and most of the electrons (upstream and downstream of the double layer) are Maxwellian. In all cases an upstream electron beam has not been observed, despite extensive attempts to measure such a phenomenon. The downstream temperature is slightly less than the upstream one: the average upstream temperature being 5.8 eV, while 5.6 eV for downstream. A more detailed study of the electron distribution and the temperature is presently being conducted.

The electron density can be expressed as a function of the plasma potential for the electrons which are in Boltzmann equilibrium:

$$n_e = n_0 \exp \frac{e\Phi}{kT_e}, \quad (18)$$

where n_e is the electron density, n_0 the electron reference density where the potential is null, Φ is the plasma potential, and T_e the electron temperature. For such electrons, the plot

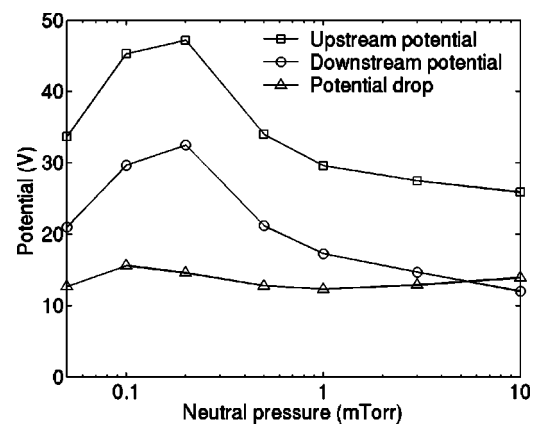


FIG. 19. Double-layer potential drop as a function of the neutral pressure.

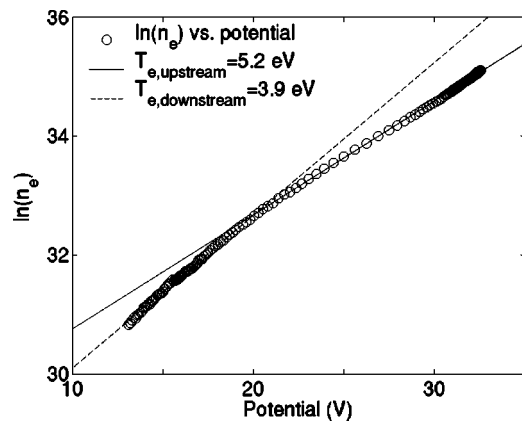


FIG. 20. Logarithm of the electron density as a function of the plasma potential.

of the natural logarithm of the electron density as a function of the plasma potential is a straight line, the slope of which yields the electron temperature. Figure 20 shows the natural logarithm of the electron density as a function of the plasma potential for a DL obtained under the standard parameters (Table I) and for a loss frequency of 10^6 s^{-1} . Two distinct parts are noticeable and obviously linear, where two linear fits are obtained with an average relative error of less than 0.5% for each one. This shows that the electrons are in Boltzmann equilibrium everywhere in the system, even across the DL. However, two electron populations coexist: a hot population upstream and within the DL, with a temperature of 5.2 eV, and a colder population downstream of the DL, with a temperature of 3.9 eV. This result is quite important and different from earlier studies: although several experimental DLs have shown two different electron temperatures, in addition to their current-driven nature, they generally present an upstream electron beam (free electrons) and do not show any clear evidence of Boltzmann electrons.^{8,44,45} It has been known that the charged particles associated with previous laboratory generated DLs may be classified into four types: free electrons, free ions, trapped electrons, and trapped ions. In general, three of these are sufficient to maintain a DL.⁴⁴ It is interesting to note that although the simulation shows a downstream ion beam (free ions, Sec. III C 2), no upstream electron beam (free electrons) has been detected despite extensive investigation. This result confirms that this type of DLs has electrons in Boltzmann equilibrium, which is rather different from the DLs which are generally simulated or are at the origin of electron acceleration in the aurora and suggests that the present DL is a different phenomenon to those previously studied.

2. Supersonic ion beam

Figure 21 represents the ion velocity distribution in phase space, where the x axis represents the position and the y axis the ion velocity. Increased brightness indicates increased density. Throughout the simulation length, we observe a low energy population of ions, which corresponds to the ions created by ionization and charge exchange collisions. Downstream of the DL a high energy population can

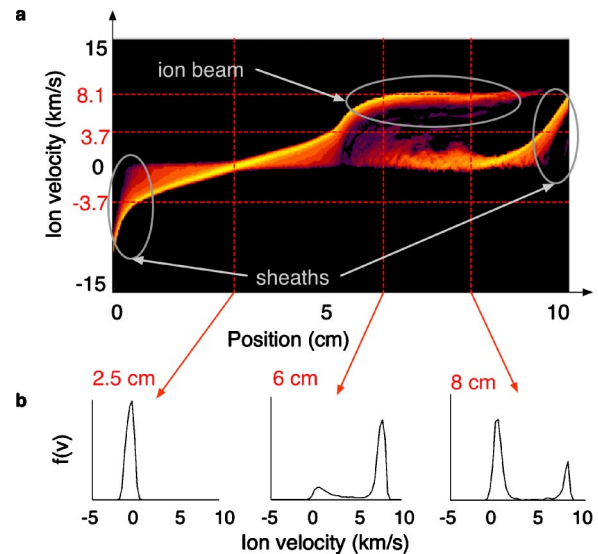


FIG. 21. (a) Ion velocity distribution in phase space, showing a supersonic ion beam. Increased brightness indicates increased density. (b) Ion velocity distribution function $[f(v)]$ in arbitrary units in different locations.

be seen, which corresponds to the ions accelerated while traversing the potential drop of the DL. The density of this ion beam decreases away from the DL as a result of ion-neutral collisions (charge exchange and elastic collisions) and of the loss process which removes fast particles as well as slow particles, as seen in Fig. 21(b). The sound speed c_s in argon for an electron temperature of 5.8 eV (upstream effective temperature) is 3.7 km/s [Eq. (9)]. Figure 21(a) shows that there is a presheath upstream of the DL that accelerates the ions up to the sound speed. As soon as the ion flow becomes supersonic, the DL appears and the ions are then accelerated up to twice the sound speed (the average velocity of the ion beam is 8.1 km/s) after less than 20 Debye lengths. The DL appears to be a detached sheath that behaves like a normal wall sheath.

IV. CONCLUSION

In this paper we have shown that a DL can be formed in a 1D-3V simulation of an expanding plasma. A new heating mechanism for 1D PIC simulation has been introduced and has shown that it does not introduce any noticeable pathologies in the spatial distribution of the plasma potential or the electron transport. The expansion rate (i.e., loss frequency) has been shown to be a critical parameter concerning the formation of the DL. This particular DL is current free and has electrons in Boltzmann equilibrium, which is rather different from all the DLs which have been simulated before. Finally we showed that the DL generates a supersonic ion beam.

¹M. Raadu, Phys. Rep. **178**, 25 (1989).

²H. Alfvén, Tellus **10**, 104 (1958).

³R. D. Albert and P. J. Lindström, Science **170**, 1398 (1970).

⁴M. Temerin, K. Cerny, W. Lotko, and F. Mozer, Phys. Rev. Lett. **48**, 1175 (1982).

⁵B. Quon and A. Wong, Phys. Rev. Lett. **37**, 1393 (1976).

⁶P. Coakley, N. Hershkovitz, R. Hubbard, and G. Joyce, Phys. Rev. Lett. **40**, 230 (1978).

- ⁷S. Torven and L. Lindberg, *J. Phys. D* **13**, 2285 (1980).
- ⁸C. Hollenstein, M. Guyot, and E. Weibel, *Phys. Rev. Lett.* **45**, 2110 (1980).
- ⁹N. Sato, R. Htakeyama, S. Iizuka, and K. Saeki, *Phys. Rev. Lett.* **46**, 1330 (1981).
- ¹⁰M. Guyot and C. Hollenstein, *Phys. Fluids* **26**, 1596 (1983).
- ¹¹C. Chan, N. Hershkowitz, A. Ferreira, T. Intrator, B. Nelson, and K. Lonngren, *Phys. Fluids* **27**, 266 (1984).
- ¹²G. Hairapetian and R. Stenzel, *Phys. Rev. Lett.* **65**, 175 (1990).
- ¹³G. Hairapetian and R. Stenzel, *Phys. Fluids B* **3**, 899 (1991).
- ¹⁴R. Hatakeyama, Y. Suzuki, and N. Sato, *Phys. Rev. Lett.* **50**, 1203 (1983).
- ¹⁵S. S. Hasan and D. Ter Haar, *Sol. Phys.* **56**, 89 (1978).
- ¹⁶S. Iizuka, K. Saeki, N. Sato, and Y. Hatta, *Phys. Rev. Lett.* **43**, 1404 (1979).
- ¹⁷S. Torven, *Phys. Rev. Lett.* **47**, 1053 (1981).
- ¹⁸G. Knorr and C. Goertz, *Astrophys. Space Sci.* **31**, 209 (1974).
- ¹⁹C. Goertz and G. Joyce, *Astrophys. Space Sci.* **32**, 165 (1975).
- ²⁰G. Joyce and R. Hubbard, *J. Plasma Phys.* **20**, 391 (1978).
- ²¹D. Newman, M. Goldman, R. Ergun, and A. Mangeney, *Phys. Rev. Lett.* **87**, 255001 (2001).
- ²²F. Perkins and Y. Sun, *Phys. Rev. Lett.* **46**, 115 (1981).
- ²³D. Trevor, N. Sadeghi, T. Nakano, J. Derouard, R. Gottscho, P. Dow Foo, and J. Cook, *Appl. Phys. Lett.* **57**, 1188 (1990).
- ²⁴C. Charles, R. W. Boswell, A. Bouchoule, C. Laure, and P. Ranson, *J. Vac. Sci. Technol. A* **9**, 661 (1991).
- ²⁵N. Sadeghi, T. Nakano, D. Trevor, and R. Gottscho, *J. Appl. Phys.* **70**, 2552 (1991).
- ²⁶T. Nakano, N. Sadeghi, D. Trevor, R. Gottscho, and R. Boswell, *J. Appl. Phys.* **72**, 3384 (1992).
- ²⁷C. Charles and R. Boswell, *Appl. Phys. Lett.* **82**, 1356 (2003).
- ²⁸C. Charles, *Appl. Phys. Lett.* **84**, 332 (2004).
- ²⁹C. Charles and R. Boswell, *Phys. Plasmas* **11**, 1701 (2004).
- ³⁰S. A. Cohen, N. Siefert, S. Stange, E. Scime, and F. Levinton, *Phys. Plasmas* **10**, 2593 (2003).
- ³¹X. Sun, C. Biloiu, R. Hardin, and E. E. Scime, *Plasma Sources Sci. Technol.* **13**, 359 (2004).
- ³²P. Hackenberg, G. Mann, and E. Marsch, *Space Sci. Rev.* **87**, 207 (1999).
- ³³B. de Pontieu, R. Erdelyi, and S. James, *Nature (London)* **430**, 536 (2004).
- ³⁴C. Birdsall and D. Fuss, *J. Comput. Phys.* **3**, 494 (1969).
- ³⁵A. Langdon and C. Birdsall, *Phys. Fluids* **13**, 2115 (1970).
- ³⁶R. Hockney and J. Eastwood, *Computer Simulation Using Particles* (IOP, Bristol, 1988).
- ³⁷C. Birdsall and A. Langdon, *Plasma Physics via Computer Simulation* (IOP, Bristol, 1991).
- ³⁸H. Skullerud, *J. Phys. D* **1**, 1567 (1968).
- ³⁹V. Vahedi and M. Surendra, *Comput. Phys. Commun.* **87**, 179 (1995).
- ⁴⁰D. Vender, Ph.D. thesis, Research School of Physical Science and Engineering, Australian National University, 1990.
- ⁴¹D. Vender and R. Boswell, *IEEE Trans. Plasma Sci.* **18**, 725 (1990).
- ⁴²M. Lieberman and A. Lichtenberg, *Principles of Plasma Discharges and Materials Processing* (Wiley-Interscience, New York, 1994).
- ⁴³P. Coakley and N. Hershkowitz, *Phys. Fluids* **22**, 1171 (1979).
- ⁴⁴C. Chan and N. Hershkowitz, *Phys. Fluids* **26**, 1587 (1983).
- ⁴⁵K. Baker, N. Singh, L. Block, R. Kist, W. Kampa, and H. Thiemann, *J. Plasma Phys.* **26**, 1 (1981).